AN ABSTRACT OF THE THESIS OF

Luc Bouchard for the degree of Master of Science in Computer Science presented on June 2, 2021.

Title: Kalman Filter Tracking for an FSO Communication System based on Dynamic Beam Steering and Shaping

Abstract approved: _____

Thinh Nguyen

We present a theoretical free-space optical (FSO) transmitter that utilizes a dynamically steered and shaped laser beam to communicate with a randomly moving receiver adorned with a retroreflector. The transmitter tracks the receiver's position by repeatedly scanning the field of view (FOV), measuring reflections from the retroreflector, and estimating the receiver's position with a Kalman filter. The transmitter sends data to the receiver in between scans. A monte-carlo simulation is used to determine the optimal FOV subsection to scan at each time step so that time spent scanning is minimized without compromising link reliability. The feasibility of the communication system is evaluated with a hypothetical implementation based on real hardware.

Kalman Filter Tracking for an FSO Communication System based on Dynamic Beam Steering and Shaping

by

Luc Bouchard

A THESIS

submitted to

Oregon State University

in partial fulfillment of
the requirements for the
degree of

Master of Science

Presented June 2, 2021
Commencement June 2021

Master of Science thesis of Luc Bouchard presented on June 2, 2021

APPROVED:

Major Professor, representing Computer Science

Head of the School of Electrical Engineering and Computer Science

---

Dean of the Graduate School

I understand that my thesis will become part of the permanent collection of Oregon State University libraries. My signature below authorizes release of my thesis to any reader upon request.

Luc Bouchard, Author

ACKNOWLEDGEMENTS

Thank you to Cade Trotter, Hayden Bialek, Alan Wang, and Arun Natarajan for your work on this project.

Thank you to my advisor, Thing Nguyen, for your guidance over the last two years.

Finally, thank you to my family and friends for supporting me on this journey when things were hard.

TABLE OF CONTENTS

KALMAN FILTER TRACKING FOR AN FSO COMMUNICATION SYSTEM BASED ON DYNAMIC BEAM STEERING AND SHAPING

1. INTRODUCTION

In just a few decades, wireless communication transformed from a niche technology to a ubiquitous tool. This expansion did not come easily—as data demands increased, available radio spectra rapidly diminished, motivating increasingly complex communications infrastructure that utilizes bandwidth with extreme efficiency [1].

Free space optical (FSO) communications systems offer an opportunity to reduce strain on the RF spectrum, opening up gigahertz of unregulated bandwidth. However, since FSO communications systems require line-of-sight (LOS), they are significantly more prone to link disruption and consequently present a host of design challenges [2].

There is widespread literature on the potential use-cases of FSO communications systems. Proposed applications include high-speed trains [3], unmanned-arial vehicles [4], building-to-building communication [5], satellite communication [6], indoor communications [7], and more [2].

In this paper, we consider a laser-based FSO transmitter that leverages beam steering and shaping technology to dynamically point a high-power, narrow beam at a mobile receiver. Using a narrow beams increases the received power, enabling faster data transmission. However, maintaining a consistent optical link with such a beam requires an accurate estimate of the receiver's location. The transmitter determines this location by scanning its beam over a grid of angular positions and measuring reflections from a

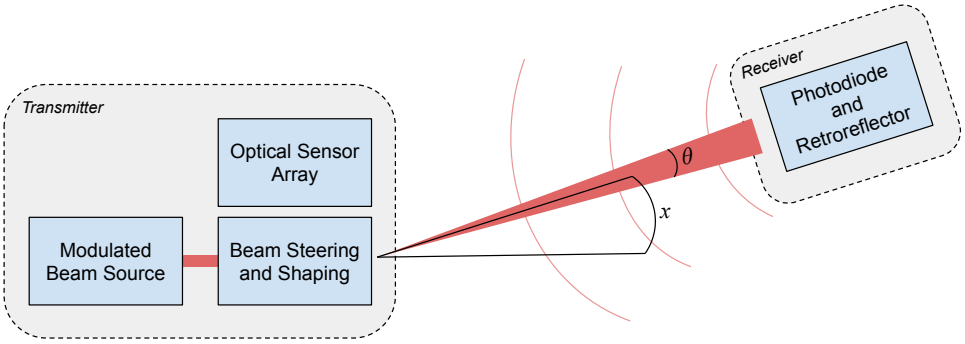

FIGURE 1.1: A one-dimensional depiction of the FSO communication system. The transmitter points a modulated laser beam along an angle, x, with a beam divergence, θ. The beam reflects off a retroreflector mounted on the receiver. The optical sensor array measures the reflected light, allowing the transmitter to locate the receiver in the FOV.

retroreflector adjacent to the receiver's photodetector. A high-level depiction of this system is shown in Fig. 1.1.

This work assumes the receiver moves along a random path without regard of the transmitter. This means the transmitter must make repeated measurements of the receiver's location to consistently send it data, and thus the transmitter's time is split between scanning the field of view (FOV) and sending data to the receiver. The beam shaping mechanism allows the transmitter to widen the beam during transmission to account for location estimate error and receiver motion.

Since the duration of a scan is proportional to the number of angular positions included in the scan grid, data transmission is maximized when the transmitter scans the smallest possible subsection of the FOV that doesn't repeatedly miss the receiver. In this paper, we present a Kalman-filter-based algorithm to track the receiver in the FOV. We then use a Monte Carlo simulation to determine the optimal scan area that minimizes scanning time and maximizes transmission.

To demonstrate feasibility, we consider an indoor application of this system using real hardware. Specifically, we assume the transmitter is mounted on the ceiling sending data to mobile receivers below. Although we focus on this use case, the proposed FSO

communication system could find applications in other settings where either the transmitter or receiver are moving along a random path. For example, mobile vehicle communication or building-to-building communication (where the transmitter and receiver are subject to building sway) could benefit from this design.

2. RELATED WORK

The problem of pointing a narrow, high-power, modulated, optical beam into a mobile receiver has been widely studied. [8] and [6] discuss a satellite-to-satellite FSO communication scheme where two satellites with precisely aligned transmit and receive paths use an ephermeris to point high-power beams at each other. One satellite then performs a spiral scan until the other satellite detects the beam, a processes referred to as acquisition. After acquisition, the satellites use a CCD image sensor to determine the angular offset of the incoming beam, enabling constant measurement of the pointing error [8].

[9] discusses the benefits of using different scanning patterns for this satellite-to-satellite acquisition process. [10] and [11] use a Monte Carlo simulation to determine the optimal area to scan to minimize the expectation value of acquisition time. While this approach is similar to the one discussed in this paper, it's only concerned with initial acquisition. It does not consider using repeated scans to track the receiver and facilitate communication.

[12] and [5] discuss the optimal beam divergence for building-to-building communication where the FSO transmitter and receiver are fixed in place but subject to building sway and vibrations. A probabilistic model of the pointing error is used to find the beam divergence that minimizes power loss while avoiding random signal dropouts. While this approach is similar to this work in that it assumes random receiver motion,

the beam itself is not dynamically steered, setting it apart from the system discussed below.

3. SYSTEM OVERVIEW

Fig. 1.1 depicts a one-dimensional representation of the proposed FSO communication system. The beam steering and shaping module controls the laser beam's divergence angle and direction, θ and x, respectively. The beam is assumed to be Gaussian. When the beam is pointed at the receiver, a retroreflector adjacent to the receiver's photodiode diffusely reflects the beam back to the transmitter. An optical sensor array mounted on the transmitter measures these reflected signals, allowing the transmitter to determine the angular location of the receiver by scanning the FOV.

3.1. Receiver

The receiver is assumed to move in the FOV with 2D continuous-time white noise angular acceleration [13]. Specifically, if $\mathbf{x} = [x \;\; y]^T$ is a 2D state vector representing the angular position of the receiver in the FOV, we assume the following relationship

$$\ddot{\mathbf{x}} = \mathbf{w}(t) \tag{3.1}$$

where $\mathbf{w}(t)$ is continuous-time Gaussian white noise with power spectral density (PSD) q. This model assumes that the receiver is approximately a fixed distance away from the transmitter, and so the horizontal and vertical angular acceleration can be sampled from a constant Gaussian distribution. If the transmitter is mounted on the ceiling communicating with users below, this is a reasonable assumption. More advanced analysis could model receivers as a 3D random walk, but this was avoided in pursuit of

simplicity.

3.2. Scanning

As mentioned above, the transmitter's time is split between two activities—transmitting data and scanning the FOV to determine the location of the receiver. Since, in general, the width of the beam used to scan could be smaller than the retroreflector, an entire image of reflection data is obtained before estimating the receiver's location. An example of such an image, along with a picture of the corresponding retroreflector, is shown in Fig. 3.1. The image was created by pointing a laser at a set of hexagonally arranged angular positions and taking reflection data at each point. The hexagonal lattice maximizes the packing efficiency of the circular beams.

Since each pixel in the scan is taken sequentially, the total scanning time is proportional to the number of pixels in the scan, n. The scan time, t_s, is given by

$$t_s = nt_p \approx \frac{2\sqrt{3}(\pi r^2)}{3\theta^2} t_p \tag{3.2}$$

where r is the angular radius of the scan, θ is the divergence angle of the beam, and t_p is the time required for each pixel. The approximation for n is derived in section 8.1. To simplify Eq. (3.2), we introduce a constant, α, which we define as the scanning speed

$$\alpha = \frac{\sqrt{3}\theta^2}{2t_p} \qquad\qquad t_s = \frac{\pi r^2}{\alpha} \tag{3.3}$$

Between scans, the transmitter sends data to the receiver. In this work, we assume the time spent transmitting is a fixed duration, t_c. In general, this quantity could change dynamically to create a more flexible system. However, here it is assumed a fixed algorithmic parameter to simplify analysis. A discussion of how t_c is selected in given in section 3.4.. Given t_c, we define the time between subsequent scans, Δt,

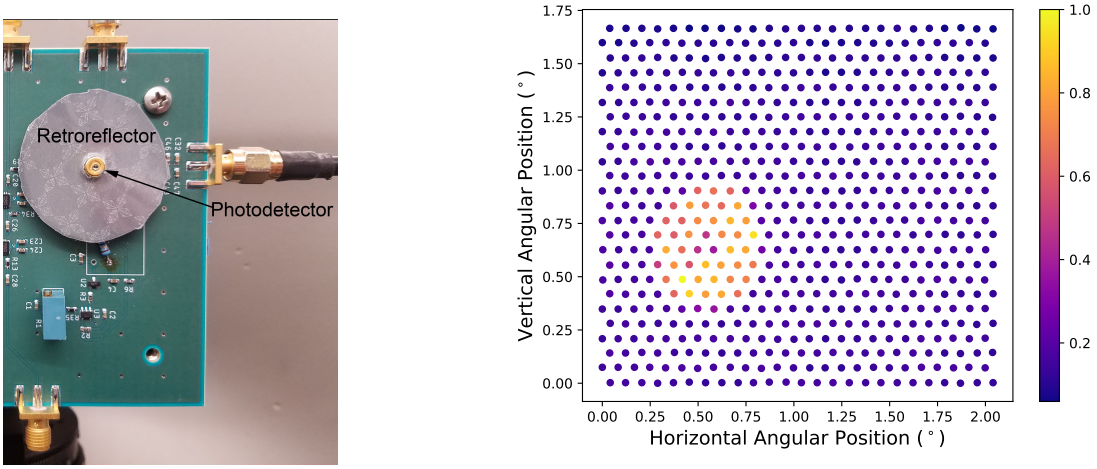

(a) (b)

FIGURE 3.1: (a) A donut-shaped retroreflector along with (b) normalized reflection data produced by scanning a 0.2° divergent beam in a hexagonal pattern over the retroreflector, which was 3 meters from the transmitter. Regions of high reflectivity have a value of approximately one. The donut is clearly visible in the bottom left corner.

$$\Delta t = t_s + t_c \tag{3.4}$$

3.3. Measurement

To convert a scan image like the one in Fig. 3.1b into a position measurement, we employ a centroid algorithm. If the scan image is given by a function $f(\mathbf{x})$, where $\mathbf{x}$ is a 2D vector representing an angular position, we first map each point in the image to 0 or 1 given a threshold value, c,

$$g(\mathbf{x}) = \begin{cases} 0 & \text{if } f(\mathbf{x}) < c \\ 1 & \text{otherwise} \end{cases} \tag{3.5}$$

The position measurement, $\mathbf{z}$, is then given by

$$\mathbf{z} = \frac{1}{N} \sum_{\mathbf{x} \in X} \mathbf{x} g(\mathbf{x}) \tag{3.6}$$

where X is the set of angular positions used in the scan, and N is the number of non-zero points

$$N = \sum_{\mathbf{x} \in X} g(\mathbf{x}) \tag{3.7}$$

In other words, the measurement, $\mathbf{z}$, is the average position of all pixels with a value larger than c. $\mathbf{z}$ is assumed to include additive Gaussian noise. The sources of this noise are two fold. The first source comes from inaccuracies in this algorithm. Since the reflection data is noisy and the receiver could be moving during the scan, the centroid position is imprecise. This is modeled as zero-mean additive Gaussian noise with standard deviation σ_c.

The second source of measurement noise comes from the duration of the scan. If the scan covers a large angular area, the receiver will have moved by the time the scan completes, introducing error into the measurement. Since larger scan areas take longer to complete, this error increases with the angular area of the scan. This error is modeled as zero-mean additive Gaussian noise with standard deviation σ_m

$$\sigma_m = \sqrt{\frac{q t_s^3}{3}} \tag{3.8}$$

where q is power spectral density of the receiver model, and t_s is the duration of the scan. This relationship is the position variance of a continuous-time white noise acceleration model propagated over a time interval t_s [14].

Since the sources of error are both zero-mean Gaussian noise and are independent of each other, the total measurement noise is also zero-mean Gaussian noise with variance σ_h^2

$$\sigma_h^2 = \sigma_c^2 + \sigma_m^2 \tag{3.9}$$

3.4. Transmission Time

For continuous communication, the receiver must be within the width of modulated beam for the duration of the transmission time, t_c. Using Eq. 3.8, we can determine the angular position variance, σ_p, of the user after this time interval

$$\sigma_p = \sqrt{\frac{qt_c^3}{3}} \tag{3.10}$$

Adding σ_p^2 to the measurement noise from Eq. 3.9, σ_h^2, leads to an upper-bound on the variance of the receiver position estimate over the time interval t_c. As long as this value is smaller than half the divergence angle of the transmission beam, θ, then the receiver will be within the beam width most of the time

$$\frac{\theta}{2} < \sqrt{\sigma_p^2 + \sigma_h^2} = \sqrt{\frac{qt_c^3}{3} + \frac{qt_s^3}{3} + \sigma_c^2} \tag{3.11}$$

A comprehensive discussion of the optimal transmission beam divergence, θ, and transmission time, t_c, is beyond the scope of this paper. Relevant analysis can be found in [12] and [5]. In this work, we simply choose an arbitrary t_c that meets the criteria given in Eq. 3.11.

4. SCANNING ALGORITHM

To choose the best region to scan, the scanning algorithm maintains an estimate of the receiver state. This is represented as a 4D state vector $\mathbf{x} = [x \;\; \dot{x} \;\; y \;\; \dot{y}]^T$ where x and

y are the horizontal and vertical angular positions of the receiver, respectively. Over a fixed time interval, Δt, this state vector evolves according to the following

$$\mathbf{x}_{k+1} = F\mathbf{x}_k + \mathbf{w}_k \tag{4.1}$$

where $\mathbf{w}_k$ is Gaussian white noise and F is the state transition matrix, given by

$$F = \begin{bmatrix} 1 & \Delta t & 0 & 0 \\ 0 & 1 & 0 & 0 \\ 0 & 0 & 1 & \Delta t \\ 0 & 0 & 0 & 1 \end{bmatrix} \tag{4.2}$$

At each time t_k, the measured receiver position $\mathbf{z}_k$ is modeled as

$$\mathbf{z}_k = H\mathbf{x}_k + \mathbf{v}_k \tag{4.3}$$

where $\mathbf{v}_k$ is Gaussian white noise and H is the observation matrix

$$H = \begin{bmatrix} 1 & 0 & 0 & 0 \\ 0 & 0 & 1 & 0 \end{bmatrix} \tag{4.4}$$

For this system, the optimal estimator of the state vector, $\mathbf{x}_k$, using measurements $\mathbf{z}_k$, $\mathbf{z}_{k-1}$, $\mathbf{z}_{k-2}$, ..., $\mathbf{z}_0$ is the Kalman filter [14]. For a continuous-time while noise acceleration model, the Kalman filter's process noise matrix is

$$Q = \begin{bmatrix} \Delta t^3/3 & \Delta t^2/2 & 0 & 0 \\ \Delta t^2/2 & \Delta t & 0 & 0 \\ 0 & 0 & \Delta t^3/3 & \Delta t^2/2 \\ 0 & 0 & \Delta t^2/2 & \Delta t \end{bmatrix} q \tag{4.5}$$

The Kalman filter's measurement noise matrix is

$$R = \begin{bmatrix} 1 & 0 \\ 0 & 1 \end{bmatrix} \sigma_h^2 \tag{4.6}$$

where σ_h is a function of the scanning time t_s, as discussed in section 3.3. [14]. The Kalman filter provides an estimate of the location and velocity of the user at any point in time.

When performing a scan, the transmitter uses the Kalman filter state estimate to decide the center of the scan. The angular radius of the scan is given by a constant, pre-determined algorithmic parameter r. Thus, the scan area is constant throughout tracking. The transmitter first computes the scan duration using the scanning speed, α. The scan is then centered on the receiver's predicted location halfway through the scan, which is computed by running the predict step of the Kalman filter with a time step equal to half the scan duration. This process is outlined in Alg. 1.

Algorithm 1 Obtain a location measurement.

Input: State vector $\mathbf{x}$, transition matrix F, scan radius r

Output: Location measurement $\mathbf{z}$

$\mathbf{c} \leftarrow F\mathbf{x}$ with $\Delta t = t_s/2$

$I \leftarrow$ Scan image with radius r and center $\mathbf{c}$

$\mathbf{z} \leftarrow$ Centroid of I

If the scan successfully returns a location measurement, the transmitter updates the Kalman filter state and switches into transmission mode. If the scan misses, the transmitter propagates the filter state forward without a measurement and repeats the scan.

Excessively small values for r lead to scans that repeatedly miss the user, resulting in poor system performance. However, unnecessarily large r values mean the transmitter is wasting time scanning more area than necessary, also degrading system performance.

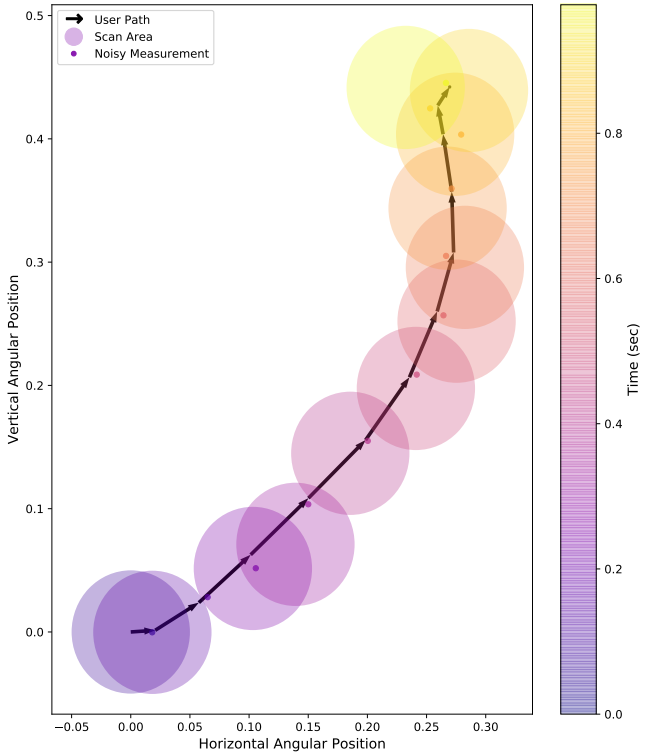

FIGURE 5.1: A one-second run of the simulation framework. The arrows represent the receiver's path, and the large colored circles are the area scanned when the receiver was at the base of the arrow. The small colored circles are the noisy measurement obtained from each scan. $r = 0.1$, $q = 2$, $\sigma_c = 0.005$, $\alpha = 1$, $t_c = 0.05$, $t_{max} = 1$.

The optimal r is found through Monte Carlo simulation, as discussed in the following section.

5. SIMULATION

Fig. 5.1 shows an example run of the simulation framework. The user's path is generated using the model discussed in section 3.1. and always begins at the origin. The

Kalman filter is initialized with a zeroed state vector and a diagonal covariance matrix. At each simulation time step, a scan is performed according to Alg. 1. The scan is deemed a "hit" if the receiver is in the scan area for the duration of the scan. If the scan results in a hit, it returns a location measurement with additive Gaussian noise according to the measurement model discussed in section 3.3..

5.1. Simulation Termination

While, in general, these simulations could run indefinitely, they are terminated for two reasons:

1. The scan misses five times in a row.
2. The simulation time exceeds an arbitrarily chosen maximum, t_{max}. In Fig. 5.1, $t_{max} = 1$ sec.

The termination time of a simulation is notated as t_{term}.

5.2. Performance Metrics

There are three metrics used to evaluate the performance of the simulated scanning algorithm: mean-squared error (MSE), average simulation duration, and transmission ratio. MSE is a quantity widely utilized in the tracking literature, defined as

$$MSE = E[(x - \hat{x})^2] \tag{5.1}$$

where x is the true receiver position at some time step, and $\hat{x}$ is the position predicted by the Kalman filter for the same time step.

The average simulation duration, t_{avg}, quantifies the transmitter's ability to continuously track the receiver without losing it altogether. It is defined as

$$t_{avg} = E[t_{term}] \tag{5.2}$$

where t_{term} is the termination time of the simulation as defined in section 5.1.. If this value is less than t_{max}, the scanning algorithm is consistently losing the receiver in the FOV, indicating suboptimal performance.

The final performance metric is the transmission ratio, β. It expresses the proportion of time spent communicating with the receiver,

$$\beta = \frac{t_c}{t_s + t_c} = \frac{t_c}{(\pi r^2/\alpha) + t_c} \tag{5.3}$$

where t_c is the communication time, t_s is the scanning time, r is the scan radius, and α is the scanning speed. If the optical link speed is 10 Mbps, and the transmission ratio is $\beta = 0.9$, then the transmitter's effective communication speed is 9 Mbps since it's communicating 90% of the time.

5.3. Results

Assuming constant values for the scanning speed (α), communication time (t_c), receiver model power spectral density (q), centroid algorithm error (σ_c), and maximum simulation duration (t_{max}), we consider the performance impact of the scan radius parameter, r, using a Monte Carlo simulation. Fig. 5.2 shows results from performing 100 simulations at 30 different scan radii ranging from 0.005 to 0.2. Each simulation is maximum 30 seconds long ($t_{max} = 30$).

When r is small ($r < 0.25$), the scanning algorithm repeatedly misses the receiver, driving down t_{avg} and increasing the MSE of the estimate. As r increases, the algorithm

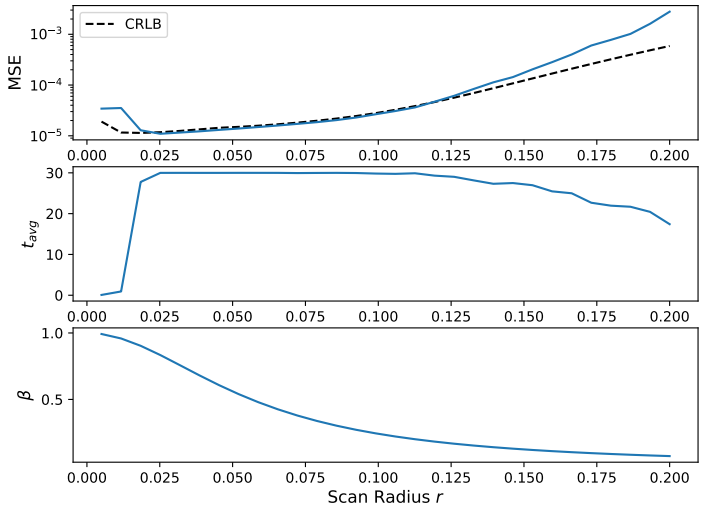

FIGURE 5.2: Monte Carlo simulation results at 30 different scan radii with 100 simulations for each radius. The simulation parameters are $\alpha = 1$, $t_c = 0.01$, $q = 1$, $\sigma_c = 0.005$, $t_{max} = 30$.

misses less frequently, and the MSE converges on the Cramer-Rao lower bound (CRLB). When r is large, the transmitter scans more area than necessary, significantly impacting the transmission ratio.

The viable values for r occur between $r = 0.25$ and $r = 0.1$. Over this interval, the transmission ratio decreases from $\beta = 0.83$ to $\beta = 0.22$.

6. FEASIBILITY WITH REAL HARDWARE

The scan data in Fig. 3.1b was produced using an experimental setup consisting of a Revibro Optics deformable MEMS mirror and a Thorlabs two-dimensional galvo beam steering system (GVSM002). This system can scan approximately 2000 angular positions per second in a hexagonal pattern ($t_p = 0.005$ sec). Using a scanning beam divergence of $\theta = 0.3°$ (0.0052 rad), the scanning speed of this system is

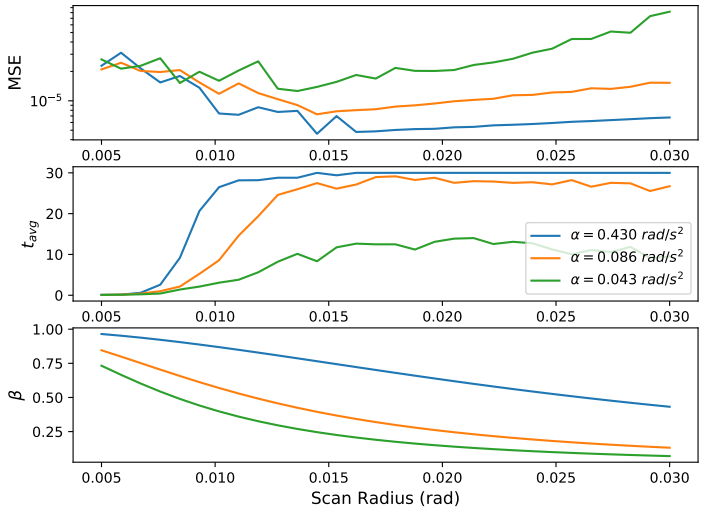

FIGURE 6.1: Monte-carlo simulation results using parameters from hardware implementation. $q = 0.1$ rad^2/Hz, $t_c = 0.005$ sec, $\sigma_c = 0.005$ rad, $t_{max} = 30$ sec. With this value for q, the average simulated receiver speed at a distance of 3 meters from the transmitter is 1.69 m/s.

$\alpha = 0.043$ rad^2/s. The centroid algorithm measurement error at this beam divergence is estimated as $\sigma_c = 0.3°$ (0.005 rad).

Assuming this transmitter is mounted on the ceiling communicating with a device in the hand of a human below, we choose the PSD, q, so that the average simulated receiver speed is consistent with human walking speed. Approximating the distance between the transmitter and receiver as 3 meters, we compute the average receiver speed for a given PSD. When $q = 0.1$ rad^2/Hz, the average speed over a 30 second interval at 3 meters distance is 1.69 m/s. Given that human walking speed is approximately 1.5 m/s [15], this PSD meets the criteria.

Fig. 6.1 shows results from a Monte Carlo simulation using these parameters. This plot also includes results when the galvo mirror scanning speed is increased by a factor of 2 and 10.

When the scanning speed is consistent with the Thorlabs galvo ($\alpha = 0.043$ rad^2/s),

the average simulation duration falls significantly short of t_{max}, indicating the system cannot consistently track the receiver. However, at double the scanning speed, ($\alpha = 0.086\ rad^2/s$), the average simulation duration comes much closer to converging on t_{max}. This performance is only further improved when the scanning speed increases by an order of magnitude, $\alpha = 0.43\ rad^2/s$.

Thus, while the experimental hardware described above is insufficient for tracking a human walking through the FOV, hardware advances that increase scanning speed could make this system feasible. This could be accomplished using a scanning pattern that is more efficient for the galvo mirror dynamics than a hexagonal raster. [9] discusses some alternative patterns like the Lissajous pattern. Scanning speed improvements could also come by replacing the galvo with a solid-state beam steering mechanism like a spatial light modulator (SLM). These devices can achieve scanning speeds upwards of ten times that of the galvo mirror [16].

7. CONCLUSION

We presented an FSO transmitter that utilizes a dynamically steered and shaped laser beam to communicate with a randomly moving receiver adorned with a retroreflector. The transmitter tracks the receiver's position by repeatedly scanning the FOV, measuring reflections from the retroreflector, and estimating the receiver's position with a Kalman filter. A Monte Carlo simulation was used to determine the optimal FOV subsection to scan at each time step so that time spent scanning is minimized without compromising link reliability.

Feasibility of the system was evaluated for a theoretical implementation based on a Revibro Optics deformable MEMS mirror and a Thorlabs two-dimensional galvo beam steering system (GVSM002). While this hardware was insufficient for communicating

with a human walking through the FOV at a distance of 3 meters, faster beam steering technology could make the system feasible.

Although this paper has provided evidence that this FSO system is theoretically possible, there are several problems left unaddressed. One such issue is angular tolerance—the receiver's photodetector and retroreflector must be reasonably well aligned with the transmission beam for communication to be possible. While this could be addressed by distributing multiple transmitters throughout a space, this comes with significant hardware costs.

Furthermore, we have not evaluated bit error rates when the receiver is in motion within the transmission beam. A model of the beam's intensity profile should be coupled with the receiver movement model to determine feasible transmission rates.

BIBLIOGRAPHY

1. A. Goldsmith, *Wireless communications*. Cambridge ; New York: Cambridge University Press, 2005.

2. Y. Kaymak, R. Rojas-Cessa, J. Feng, N. Ansari, M. Zhou, and T. Zhang, "A survey on acquisition, tracking, and pointing mechanisms for mobile free-space optical communications," *IEEE Communications surveys and tutorials*, vol. 20, no. 2, pp. 1104–1123, 2018.

3. S. Fathi-Kazerooni, Y. Kaymak, R. Rojas-Cessa, J. Feng, N. Ansari, M. Zhou, and T. Zhang, "Optimal positioning of ground base stations in free-space optical communications for high-speed trains," *IEEE transactions on intelligent transportation systems*, vol. 19, no. 6, pp. 1940–1949, 2018.

4. A. Carrasco-Casado, R. Vergaz, J. M. Sanchez-Pena, E. Oton, M. A. Geday, and J. M. Oton, "Low-impact air-to-ground free-space optical communication system design and first results," in *2011 International Conference on Space Optical Systems and Applications (ICSOS)*. IEEE, 2011, pp. 109–112.

5. S. Arnon, "Optimization of urban optical wireless communication systems," *IEEE transactions on wireless communications*, vol. 2, no. 4, pp. 626–629, 2003.

6. J. Romba, Z. Sodnik, M. Reyes, A. Alonso, and A. Bird, "ESA's bidirectional space-to-ground laser communication experiments," in *Free-Space Laser Communications IV*, J. C. Ricklin and D. G. Voelz, Eds., vol. 5550, International Society for Optics and Photonics. SPIE, 2004, pp. 287 – 298. [Online]. Available: https://doi.org/10.1117/12.560934

7. S. Liverman, Q. Wang, Y.-J. Chu, A. Borah, S. Wang, A. Natarajan, A. X. Wang, and T. Nguyen, "Wifo: A hybrid communication network based on integrated free-space optical and wifi femtocells," *Computer communications*, vol. 132, pp. 74–83, 2018.

8. G. BAISTER and P. V. GATENBY, "Pointing, acquisition and tracking for optical space communications," *Electronics and communication engineering journal*, vol. 6, no. 6, pp. 271–280, 1994.

9. M. Scheinfeild, N. S. Kopeika, and A. Shlomi, "Acquisition time calculation and influence of vibrations for microsatellite laser communication in space," in *Acquisition, Tracking, and Pointing XV*, M. K. Masten and L. A. Stockum, Eds., vol. 4365, International Society for Optics and Photonics. SPIE, 2001, pp. 195 – 205. [Online]. Available: https://doi.org/10.1117/12.438047

10. X. Li, S. Yu, J. Ma, and L. Tan, "Analytical expression and optimization of spatial acquisition for intersatellite optical communications," *Opt. Express*, vol. 19, no. 3, pp. 2381–2390, Jan 2011. [Online]. Available: http://www.opticsexpress.org/abstract.cfm?URI=oe-19-3-2381

11. J. Ma, G. Lu, L. Tan, S. Yu, Y. Fu, and F. Li, "Satellite platform vibration influence on acquisition system for intersatellite optical communications," *Optics and laser technology*, vol. 138, p. 106874, 2021.

12. M. A. Amirabadi and V. Tabataba Vakili, "A new optimization problem in fso communication system," *IEEE communications letters*, vol. 22, no. 7, pp. 1442–1445, 2018.

13. Y. Bar-Shalom, *Estimation with applications to tracking and navigation.* New York: Wiley, 2001.

14. A. J. Haug, *Bayesian estimation and tracking : a practical guide*, 1st ed. Hoboken, New Jersey: Wiley, 2012.

15. B. J. Mohler, W. B. Thompson, S. H. Creem-Regehr, H. L. Pick Jr, and W. H. Warren Jr, "Visual flow influences gait transition speed and preferred walking speed," *Experimental brain research*, vol. 181, no. 2, pp. 221–228, 2007.

16. Y. Takaki and N. Okada, "Hologram generation by horizontal scanning of a high-speed spatial light modulator," *Applied optics. Optical technology and biomedical optics*, vol. 48, no. 17, pp. 3255–3260, 2009.

8. APPENDICES

8.1. Number of Circles in Hexagonal Lattice

A hexagonal lattice fits 3 circles of diameter θ into a hexagon with side length θ. The area of such a hexagon, A_h, is given by,

$$A_h = \frac{3\sqrt{3}}{2}\theta^2 \tag{8.1}$$

Given an arbitrary area A, we can approximate the number of hexagons, n_h, we can fit in A with,

$$n_h \approx \frac{A}{A_h} = \frac{2\sqrt{3}A}{9\theta^2} \tag{8.2}$$

Multiplying n_h by the number of circles in each hexagon gives us the number of circles in A, n_c,

$$n_c = 3n_h \approx \frac{2\sqrt{3}A}{3\theta^2} \tag{8.3}$$